Supplementary Information: Enhanced and Polarization Dependent Coupling for Photoaligned Liquid Crystalline Conjugated Polymer Microcavities

Florian Le Roux,*,† Robert A. Taylor,† and Donal D. C. Bradley*,†,‡

†*Department of Physics, University of Oxford, Parks Road, Oxford, OX1 3PU, U.K.*

‡*Physical Science and Engineering Division, King Abdullah University of Science and Technology, Thuwal, 23955-6900, Saudi Arabia*

E-mail: florian.leroux@physics.ox.ac.uk; donal.bradley@kaust.edu.sa

Optical constants of non-aligned (NA) and aligned (A) LCCP films

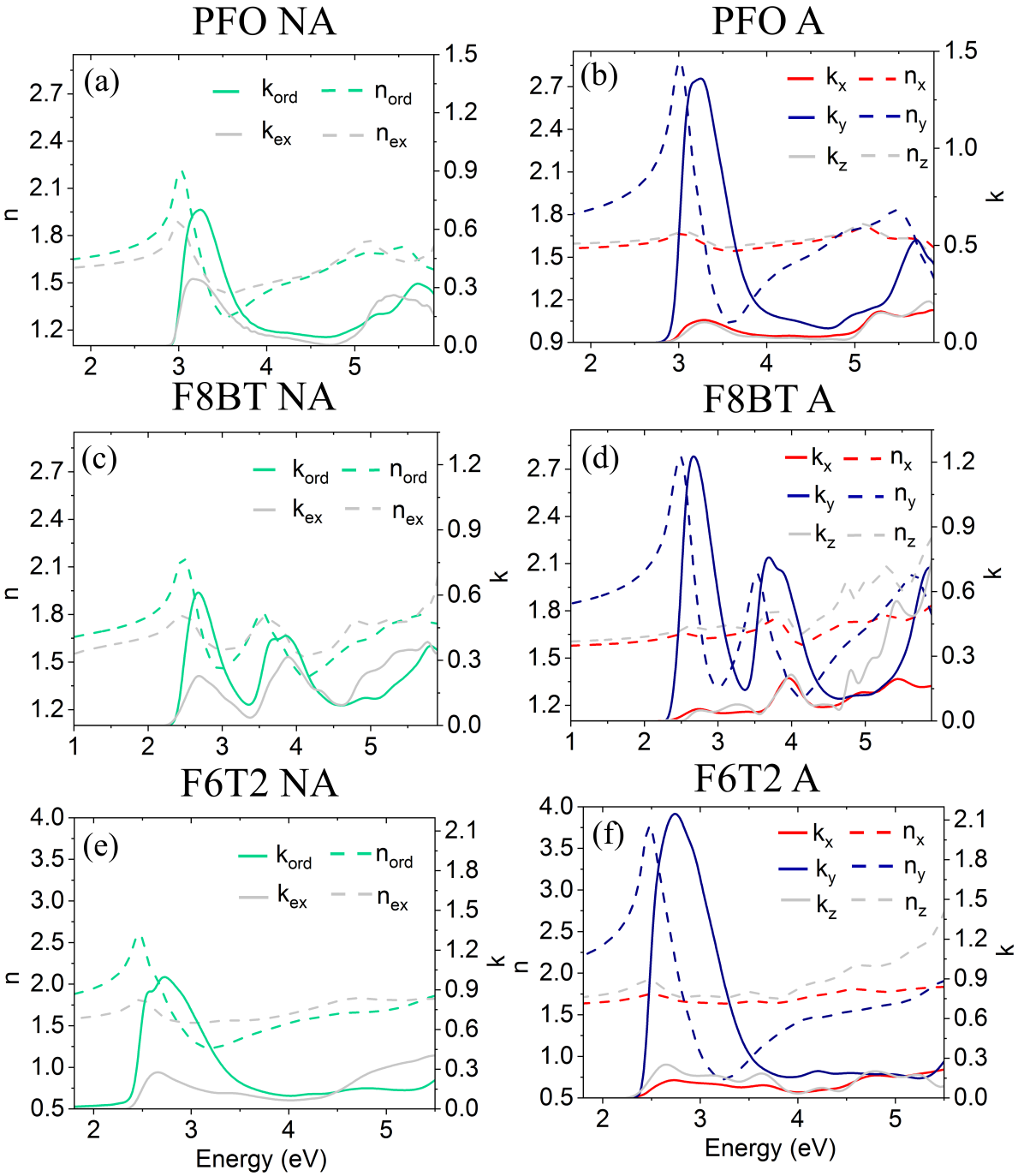

Figure S1: In green and grey respectively in-plane (n_{ord}, k_{ord}) and out-of-plane (n_{ex}, k_{ex}) optical components for non-aligned PFO (a), F8BT (c), F6T2 (e) thin films. In blue, red and grey respectively in-plane in the aligned polymer chains direction (n_y, k_y), in-plane in the direction perpendicular to the chains (n_x, k_x) and out-of plane (n_z, k_z) optical components for aligned PFO (b), F6T2 (c), F8BT (d). Dashed lines give the real component of the complex refractive index $\tilde{n} = n + ik$, solid lines the imaginary component.

Angular variation of s- and p-polarized transmittances at normal incidence for a thin film of aligned PFO

We measure the s- and p- polarized transmittances of a thin film of aligned PFO at normal incidence while rotating the sample. The sample angle is defined as the angle formed between the direction x (which is the direction of the polarizer that was used during the alignment of SD1) and the p polarization. We define the ratio:

$$R_T = \begin{cases} \frac{\int_{E_{\min}}^{E_{\max}} T_{\text{ref}} - T_s dE}{\int_{E_{\min}}^{E_{\max}} T_{\text{ref}} - T_p dE} \text{ if } \mathrm{T_s} > \mathrm{T_p}, \\ \frac{\int_{E_{\min}}^{E_{\max}} T_{\text{ref}} - T_p dE}{\int_{E_{\min}}^{E_{\max}} T_{\text{ref}} - T_s dE} \text{ if } \mathrm{T_s} \leqslant \mathrm{T_p} \end{cases} \tag{1}$$

where T_{ref} is the transmittance obtained for a quartz substrate, $E_{\min}$ and $E_{\max}$ the energies around the exciton distribution (for PFO: $E_{\min} = 2.10$ eV and $E_{\max} = 3.80$ eV). Figure S2 shows the values of R_T for sample angles ranging from $-15°$ to $105°$. Two minimas of around 0.2 are clearly observable at $0°$ and $90°$ while unity is reached precisely at $45°$. These values confirm the alignment of the average transition dipole moment along the y direction (direction perpendicular to the polarizer direction used for the alignment of SD1) and justify the use of x and y as principal coordinates.

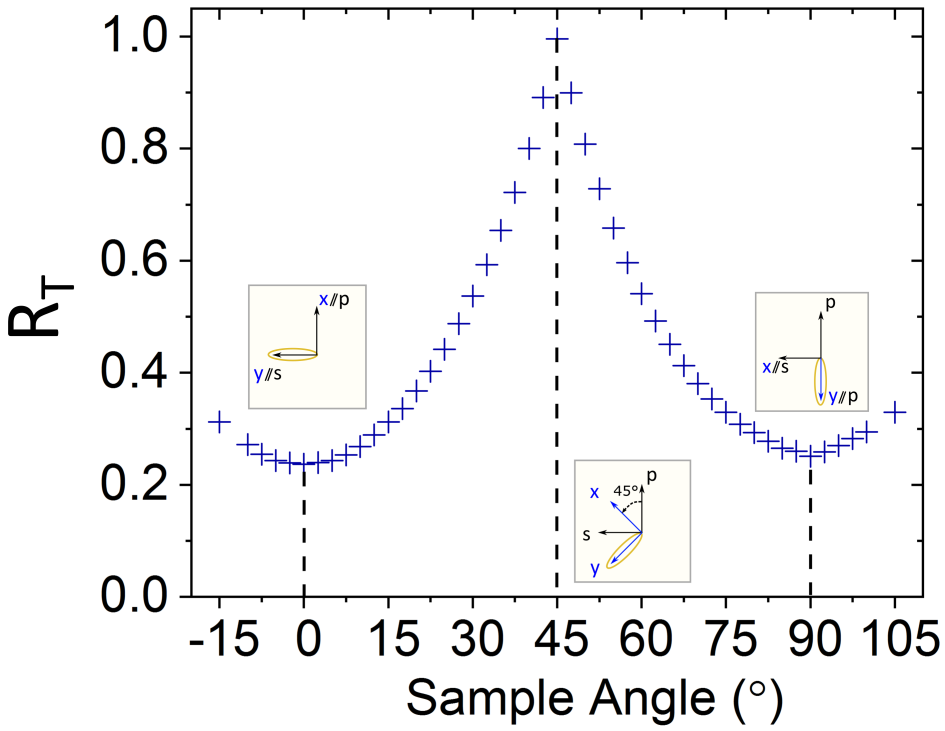

Figure S2: R_T vs sample angle as defined in text. Two minimas are clearly observed at 0° and 90° while a maximum is observed at 45°. These three specific geometries correspond to the represented experiment schematics.

Ultrastrong Coupling in Metallic Microcavities

Experimental and Analytical Results for Non-aligned F8BT and PFO

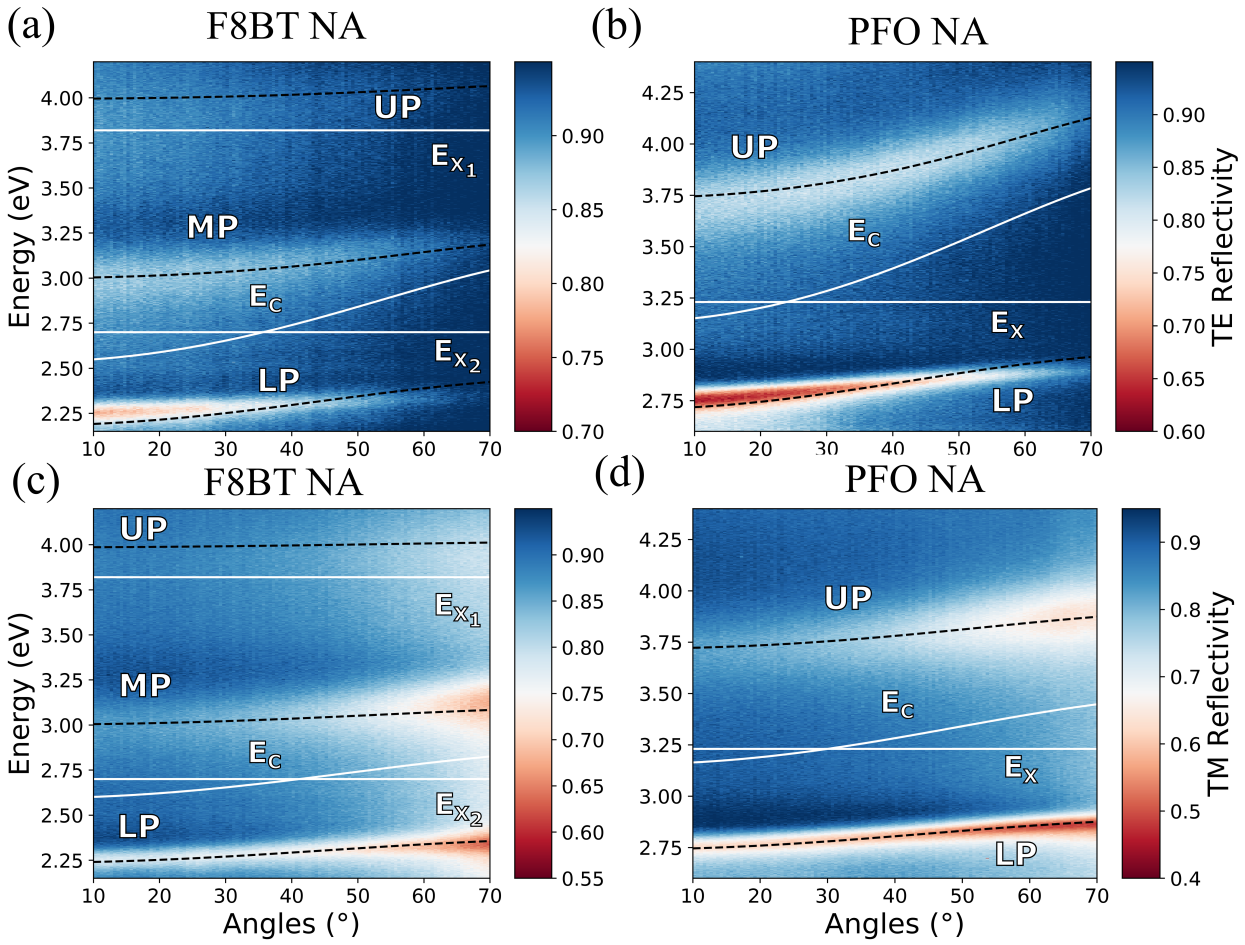

Figure S3: Experimental, angle-resolved, TE-polarized reflectivity maps for microcavities containing non-aligned F8BT (a,c) and PFO (b,d) for the TE (a,b) and TM (c,d) polarizations. Overlaid are the fitting curves obtained using the analytical model presented in Methods, the fitting values are shown in Table 1. Overlaid solid white lines are the Excitons E_{X_j} and cavity E_C modes, black dashed lines are the polaritons obtained from fitting using the analytical model.

TMR Calculations

Figure S4, S5, S6 show the results obtained from Transfer Matrix Reflectivity (TMR) calculations using the optical constants obtained in Figure S1 for F8BT (Figure S4), PFO (Figure S5) and F6T2 (Figure S6) against the corresponding experimental reflectivity measurements for all microcavities presented in this work. The thicknesses indicated are the simulated layer thicknesses for the corresponding polymer or SD1 layer. For the aligned cavities Φ is the azimuthal angle formed between the incident TE-polarization direction and the polymer chain direction.

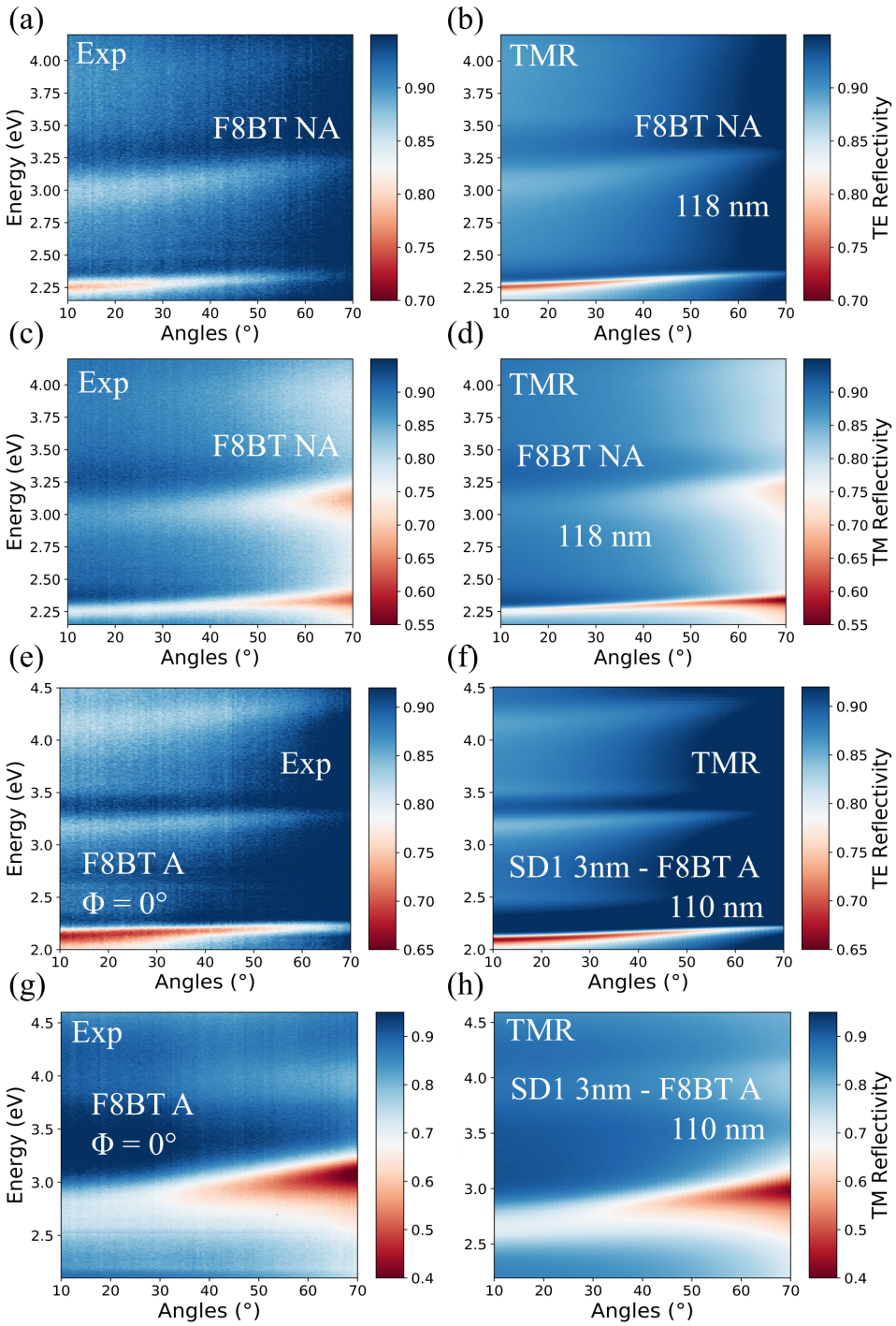

Figure S4: On the left, Experimental, angle-resolved, TE-(a,e) and TM-(c,g) polarized reflectivity maps for microcavities containing non-aligned (a,c) and aligned (e,g) F8BT. On the right, TMR calculations results showing angle-resolved, TE-(b,f) and TM-(d,h) polarized reflectivity maps for microcavities containing non-aligned (b,c) and aligned (e,g) F8BT. For the aligned cavities, the measurements and calculations were performed for $\Phi = 0°$. The thicknesses displayed in white correspond to the SD1 and polymer layer thicknesses used in the TMR calculations.

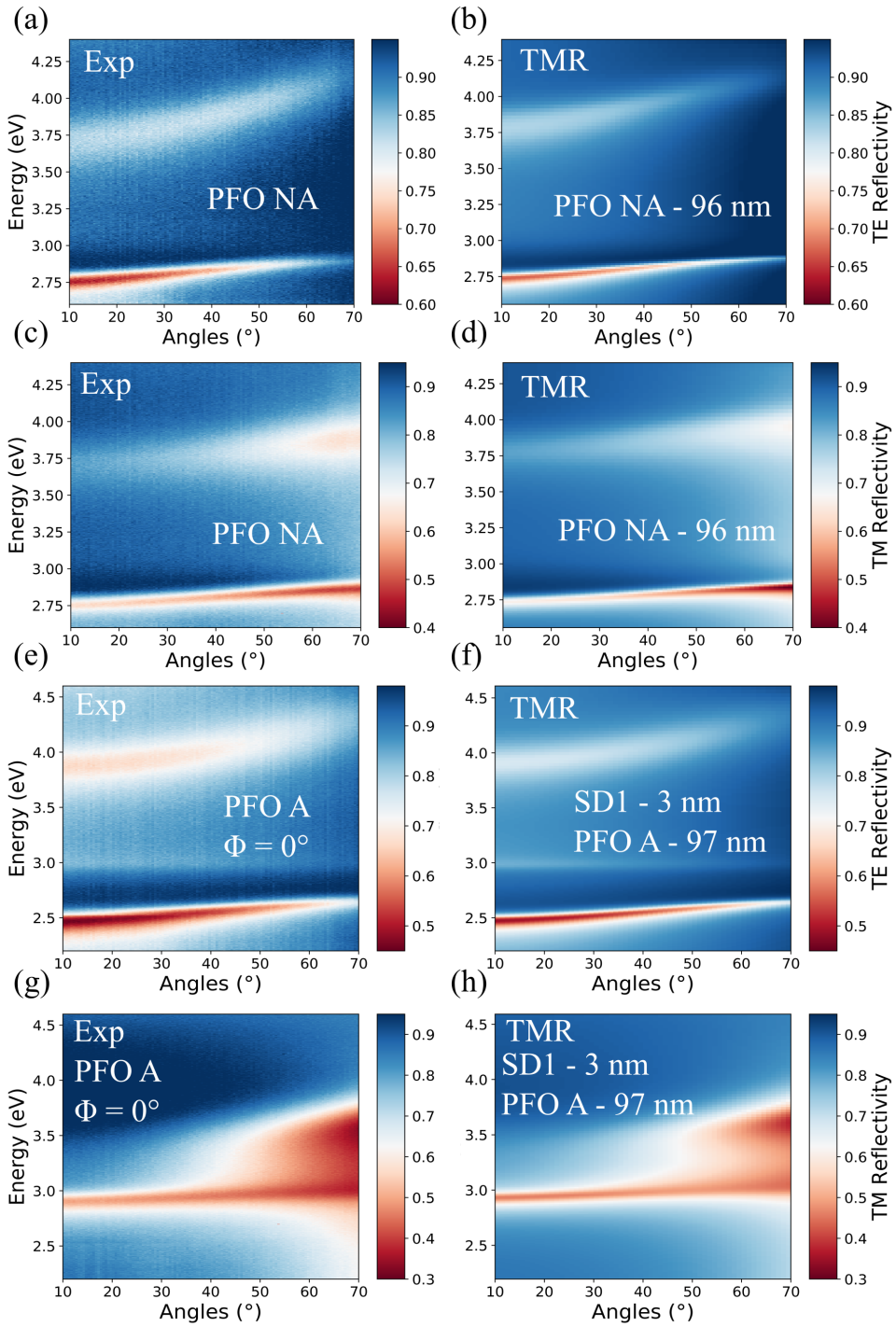

Figure S5: On the left, Experimental, angle-resolved, TE-(a,e) and TM-(c,g) polarized reflectivity maps for microcavities containing non-aligned (a,c) and aligned (e,g) PFO. On the right, TMR calculations results showing angle-resolved, TE-(b,f) and TM-(d,h) polarized reflectivity maps for microcavities containing non-aligned (b,c) and aligned (e,g) PFO. For the aligned cavities, the measurements and calculations were performed for $\Phi = 0°$. The thicknesses displayed in white correspond to the SD1 and polymer layer thicknesses used in the TMR calculations.

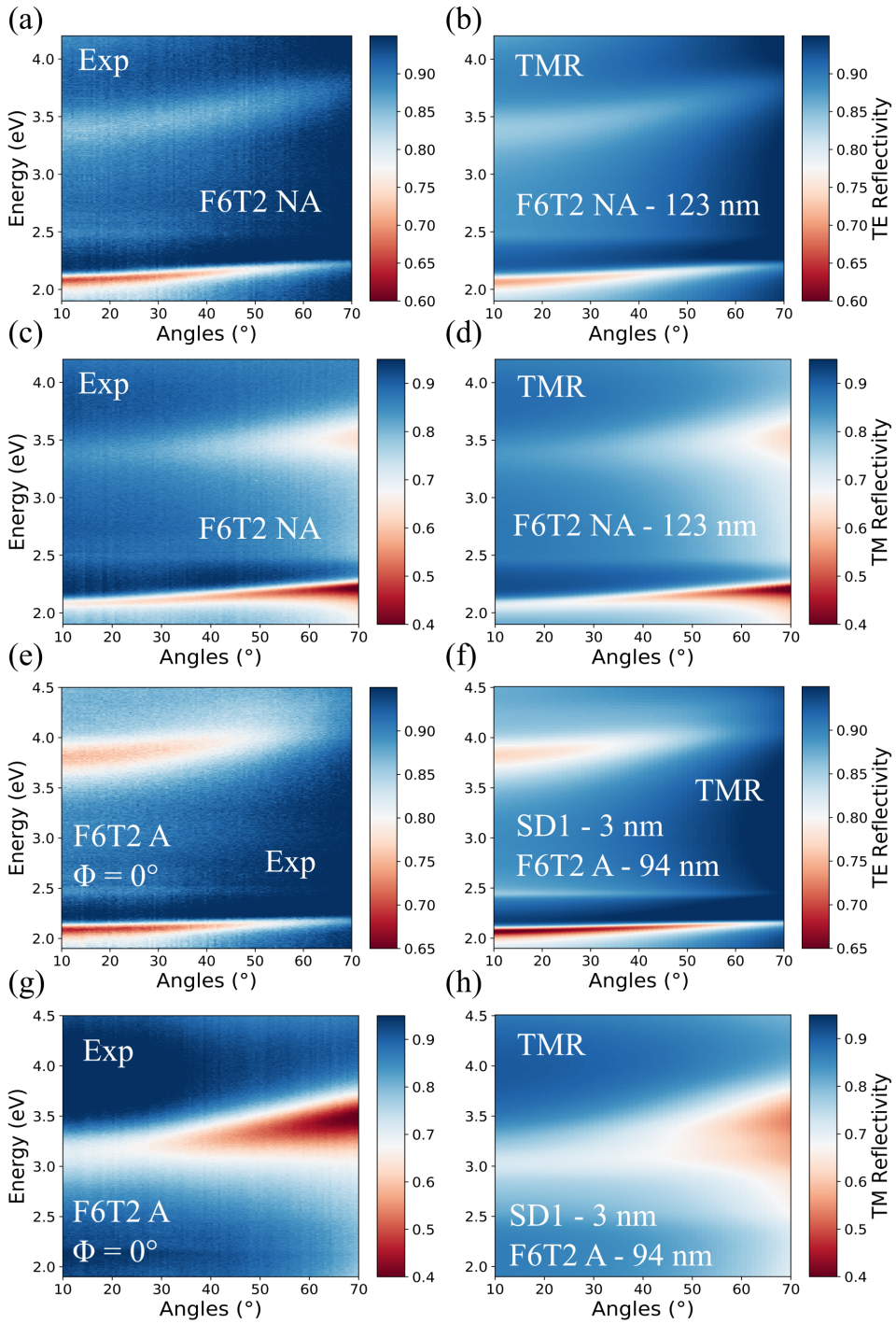

Figure S6: On the left, Experimental, angle-resolved, TE-(a,e) and TM-(c,g) polarized reflectivity maps for microcavities containing non-aligned (a,c) and aligned (e,g) F6T2. On the right, TMR calculations results showing angle-resolved, TE-(b,f) and TM-(d,h) polarized reflectivity maps for microcavities containing non-aligned (b,c) and aligned (e,g) F6T2. For the aligned cavities, the measurements and calculations were performed for $\Phi = 0°$. The thicknesses displayed in white correspond to the SD1 and polymer layer thicknesses used in the TMR calculations.